Lambert SM, Armstrong M, Wang C, Attidekou PS, Christensen P, Widmer JD, Scott K.

A rapid non-destructive-testing technique for in-line quality control of Li-ion batteries.

***IEEE Transactions on Industrial Electronics* (2016)**

http://dx.doi.org/10.1109/TIE.2016.2643601

A Rapid Non-Destructive-Testing Technique for In-Line Quality Control of Li-Ion Batteries

Simon M. Lambert, Matthew Armstrong, Pierrot Attidekou, Paul Christensen, James D. Widmer, Chen Wang and Keith Scott

***Abstract*— Quality control in the production of automotive Li-ion cells is essential for both safety and economic reasons. At present, as part of the production process, it is common practice to store Li-ion cells for up to two weeks to analyse self-discharge performance and to subject sample cells to months of cycling to assess lifetime performance. This paper presents a new state-of-the-art non-destructive testing technique for automotive scale, Li-ion batteries. Importantly, the test can discriminate between viable and non-viable cells in less than one minute. This is significantly quicker than many industrially applied techniques. The proposed method, developed in partnership with three independent Original Equipment Manufacturer (OEM) automotive li-ion cell manufacturers, uses empirical data gathered off-line for benchmarking cell response followed by a unique targeting process to reduce the test time to a level compatible with industrial manufacturing processes. The technique used is a targeted form of electrochemical impedance spectroscopy (EIS) using a commercially available potentiostat with EIS capability. The novel aspect of the research is the treatment of off-line empirical data, the construction of an empirical library database, and the development of a reliable and robust in-line test procedure. For reasons of commercial sensitivity no knowledge of the underlying chemistry of the cells is available for use. This demonstrates the functionality of the proposed method across a range of different cell technologies and its applicability to multiple battery technologies.**

***Index Terms* — Lithium batteries; Quality management; Electrochemical impedance spectroscopy;**

Manuscript received November 5, 2015; revised March 11, 2016 and June 13, 2016; accepted July 25, 2016. This work was supported in part by the European Commission under Framework Seven through the funding of project 285385 (European Lithium-ion Battery Advanced Manufacture – ELIBAMA).

S. M. Lambert, M. Armstrong, C. Wang and J. D. Widmer are with the School of Electrical Engineering, Newcastle University, Newcastle-Upon-Tyne, UK. P. A. Christensen, P. Attidekou and K. Scott are with the School of Chemical Engineering and Advanced Materials, Newcastle University, Newcastle-Upon-Tyne, UK. (M. Armstrong, Phone: +44-(0)191-208-5203; fax: +44-(0)191-208-8180; e-mail: matthew.armstrong@ncl.ac.uk).

NOMENCLATURE

BMS	Battery Management System
CCCV	Constant Current-Constant Voltage
EIS	Electrochemical Impedance Spectroscopy
ESR	Equivalent Series Resistance
EV	Electric Vehicle
HEV	Hybrid Electric Vehicle
NDT	Non Destructive Test
OCV	Open Circuit Voltage
OEM	Original Equipment Manufacturer
QC	Quality Control
SEI	Solid Electrolyte Interface
SOC	State of Charge
SOH	State of Health

I. INTRODUCTION

The production of large scale electric vehicle fleets for market is well established across North America, Europe, Eastern Asia, and increasingly in developing regions. One of the most complicated, and costly, elements of the production process is the lithium-ion battery fabrication. Individual cells are produced and packaged and then assembled into battery modules, or packs, containing many cells. Large scale battery cell production, like any production process, has a finite yield of acceptable end products. If a single cell in a battery pack fails then the entire pack must be disassembled and the failed cell removed and replaced. A single weak cell in a module consisting of hundreds, seriously affects the output power and compromises the performance of the whole module. Furthermore, the failure of battery systems in safety-critical electric systems, such as electric vehicle (EV) drive trains, can lead to performance deterioration, costly replacement, and more importantly serious hazards [1]. For this reason, there is a strong safety and economic case to perform quality control testing on all individual cells before the battery module assembly stage.

For batch production in the chemical industry quality control (QC) is usually achieved by taking a small sample from each batch and testing to ascertain overall acceptability. In battery failure analysis, it is common to perform post-mortem tests with

a tear-down test. This involves physically taking a failed cell apart to analyse problems [2, 3]. Apart from the obvious complexity of a Li-ion cell being a significant issue with QC chemical analysis of a single cell, the cell arrives off the production line in a sealed packaged state. Therefore, whilst upstream QC and failure analysis of battery constituents can be done through in-production sampling, it is impossible to chemically test the cell without breaking it open and materially damaging it; which is obviously undesirable. For this reason, non-destructive testing techniques appropriate for fully assembled cells are much preferred [4].

Any process of non-destructive testing and failure analysis must be developed in such a way that the QC test can be performed without any possibility of contributing towards the failure of the cell. Likewise, the test must have a sufficiently robust detection rate to prevent cells likely to fail from passing undetected; either further down the production line or whilst in use in an end product. Equally, since the volume of battery production is large, and is likely to increase as penetration of EV/HEVs increases, the test must not only be accurate but also timely and economically viable [5].

Production of Li-ion batteries may broadly be split into three phases. Firstly, the cells are mechanically formed through cutting, coating and stacking the electrodes. This is proceeded by electrolyte filling and sealing. The second phase of the process is the electrochemical and thermal formation cycles, following which each cell is ready for use. The final stage is the mechanical packaging of the cells into modules and/or battery packs with the inclusion of a battery management system (BMS), busbars and connectors. Given the complex nature of the process, quality control assessment is performed at multiple points in each phase. The quality control technique proposed in this paper is intended for implementation at the end of phase two of the aforementioned manufacturing process.

The current start of the art, employed in Original Equipment Manufacturer (OEM) automotive battery manufacturing facilities, for the final quality control check after thermal and electrical cycling is a self-discharge test in which cells are monitored over a period of up to two weeks in order to establish whether the self-discharge performance is within accepted tolerances. This test can be performed on every cell that is produced since it is completely passive, however it requires placing all cells into a production buffer for up to two weeks which adds time to the production process and requires large inventories of product to be kept in hiatus. Other tests include accelerated aging through cycling on a small selection of cells over several weeks [6], however, although these tests yield better information about lifetime performance, they are invasive tests and can only be performed on a sample set of cells which cannot then be released to market. Where problems arise in a batch of sample cells, which are typically manufactured around the same time, it may indicate that an entire batch of cells is susceptible to early failure. This can potentially lead to cells being recalled from market and exchanged at great expense to the industry. The need for a quick and reliable early indication of whether cells are likely to fail the accelerated aging test is therefore highly desirable. Groups of cells can then be withheld from market pending results of more vigorous testing and investigation. Whilst the need for such testing procedures is clearly understood, the development of such systems is a significant research challenge at present. State-of-the-art techniques are necessary to develop the rapid, yet reliable and robust, procedures necessary to support this rapidly evolving industry. Much of the existing literature focuses on in-situ state of charge estimation techniques; once the battery is actively in use [7–13]. Likewise, there are a significant number of innovative approaches to state of health and lifetime prediction [14–17]. Most of these techniques rely on computationally heavy signal processing techniques such as Kalman Filters, observers, and cross correlation techniques. Often, these methods are not time critical, and are carried out on a single battery application at a time which is convenient [18–20]. They are not normally designed for rapid viability testing of multiple cells, and more importantly typically not for use in mass production environments.

For this reason, this paper proposes a new innovative method of non-destructive electrochemical analysis using a “black box” approach to characterize cells which are viable. Importantly, the test does not require significant knowledge of the underlying cell chemistry. An Electrochemical Impedance Spectroscopy (EIS) based technique is used to measure the impedance of the cells and a novel, state-of-the-art, processing algorithm is used to analyse the data. The testing method uses empirical data to reliably distinguish between viable and non-viable cells and a frequency targeted approach to minimise the testing time. Results demonstrate that a test time of less than one minute is achievable. Compared to many existing test methodologies, this represents a significant improvement, and a successful research achievement.

II. Non-Destructive Test (NDT) Specification

The proposed NDT technique is intended to be a viable technique for the next generation of Li-ion battery manufacturing production lines. As such, the technique described by this paper is focused on modern state-of-the art and future production lines. The specification for the test, in consultation and approved by three major international automotive Li-ion cell manufacturers, is;

- Must be possible to use on every cell produced

Presently the self-discharge and accelerated aging tests are only performed on a small sample set of cells. This leads to faulted cells being released to market and having to be recalled at a later date. An in-line test of all cells is required.

- Must be non-destructive

If every cell is to be tested then the test itself must not adversely affect the performance of the cell. The cell must remain intact for further investigation, if required.

- Test time < 1 min

The proposed test time in this paper results from work carried out in partnership with the three automotive Li-ion cell manufacturers. The tact-rate (or rate at which cells are passed through the testing station) varies depending on each facility. However, a test time of < 1 minute is representative of their existing manufacturing facilities.

- Simple pass/fail result

The test is designed to be an in-line indication of cell faults. Cells which fail this test should be removed from the production line pending further investigation to potentially identify the exact reason for the fault – a process which may take significantly more time. Additionally, the test is developed in collaboration with three independent cell manufacturers whose underlying cell chemistries differ and are commercially sensitive. Therefore, the test must be applicable to multiple cell types/models from a range of different manufacturers using several unique production processes. Furthermore, due to commercial sensitivity, the test must be possible without significant knowledge of the underlying chemistry of each cell; this information is typically unavailable.

III. Electrochemical Impedance Spectroscopy

The constraints of NDT techniques, along with a commercially imposed lack of knowledge of the cell chemistry, render chemical analysis impossible for the purposes of this test. Therefore an electrical analysis technique is required. Electrochemical impedance spectroscopy (EIS) is a widely used experimental method to gain deeper insight into electro-chemical systems [21-23]. The general principle of EIS is to apply sinusoidal signals to the cell and measure the characteristic response from the cell; which is defined by the cell impedance. The input, or drive, signal can either be current (galvanostatic) or voltage (potentiostatic) [6]. By taking the voltage signal as the reference the complex impedance is defined as the complex ratio of the voltage signal to the current signal, including its phase shift as shown in (1);

$$Z(t) = \frac{v(t)}{i(t)} = \frac{\hat{V}\sin(\omega t)}{\hat{I}\sin(\omega t + \phi)} = |Z|\frac{\sin(\omega t)}{\sin(\omega t + \phi)} \quad (1)$$

From which;

$$Z = \frac{V}{I} = |Z|\exp(i\phi) = |Z|(\cos(\phi) + isin(\phi))$$

Where $\hat{V}$ is the peak voltage, $\hat{I}$ is the peak current, ω is the angular velocity (frequency), $|Z|$ is the absolute value of the impedance and ϕ is the phase difference between the current and voltage. Furthermore, the extrapolation of the real and imaginary parts of the impedance is given by (2) and (3);

$$Z_{\text{re}} = |Z|\cos(\phi) \quad (2)$$

$$Z_{\text{im}} = |Z|\sin(\phi) \quad (3)$$

Plotting these values on a Nyquist chart reveals the relationship between real and imaginary impedance over a specified frequency range [21]. A typical characteristic Nyquist impedance plot for a conventional Li-ion cell is shown in Fig. 1.

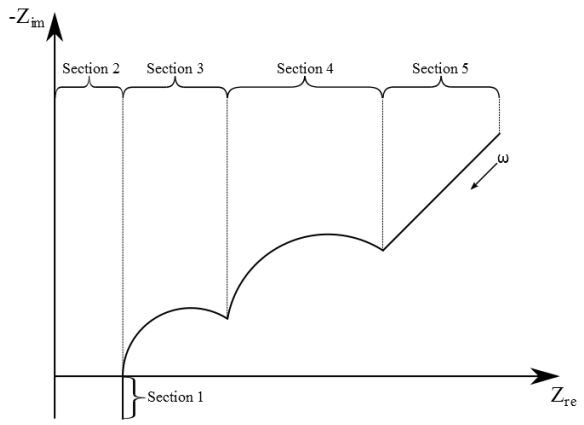

Fig. 1 - Schematic impedance spectrum in a Nyquist plot for a typical Li-ion cell [6]

In the theoretical curve shown in Fig. 1 there are five clear sections. Each semi-circular section is indicative of the impedance spectrum of an equivalent RC circuit. In [22] these sections are defined as;

Section 1 - At very high frequencies the dominant impedance is the inductive behaviour of the wire connections and any internal metal circuits [21].

Section 2 - At the intersection of the real axis there is no impedance due to reactive components; i.e. the impedance is purely Ohmic. This is the summation of the pure resistances of the active material, electrolyte and separator. This crossing point effectively gives the equivalent series resistance of the cell (ESR) [22].

Section 3 - The third section is associated with the solid-electrolyte interface (SEI) [24]. It is formed during cycling of the anode surface [25].

Section 4 - The fourth section represents the double layer capacitance and charge transfer resistance at the electrodes [26, 27].

Section 5 - As frequency approaches DC the asymptote moves off at 45° in the so called Warburg impedance [28] caused by the diffusion process in the active material [21].

When studying Li-ion batteries derivation of an equivalent circuit for the electrochemical system is common practice [9, 14, 29]. An example of an idealised equivalent circuit for a Li-ion battery is shown in Fig. 2.

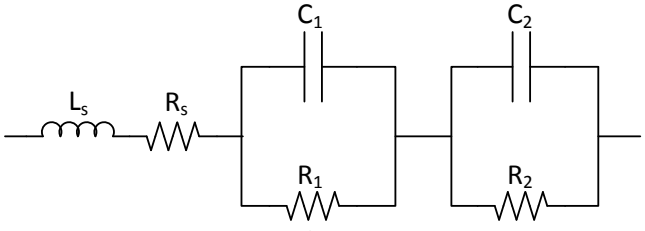

Fig. 2 - Idealised equivalent circuit for a Li-ion battery

In reality, the equivalent circuit is generally more complex employing non-physical circuit elements such as Warburg impedances and constant phase elements [29]. The equivalent circuit is a representation of the dynamic response of the cell in

much the same way as that of a transfer function. The advantage of the equivalent circuit is that it usually has circuit components which represent physical aspects of the cell chemistry or mechanical design. They are, therefore, mainly useful either for reverse engineering a cell or for identifying specific faults within a cell. Since in this work no underlying knowledge of the test cell chemistry is known the derivation of an equivalent circuit serves little purpose. Instead, use of the raw data measured from an EIS experiment gives the greatest flexibility in dynamic response analysis and ultimately leads to the ability to process the results in a timely manner.

IV. Proposed Testing Technique

In developing the proposed test, it is worth noting that three batches of cells from three different manufacturers are used. In all three cases the purpose of the proposed technique is to test all cells produced. Since the proposed test is non-destructive the test is able to be performed without harming a cell in any way, thus it can be released to market. Reassuringly, despite differences in the chemistries and manufacturing processes for each batch of cells, results are found to be consistent within each group of cells, and confirm the viability of the test. For conciseness, and to allow for a full description of the innovative technique, the results presented in this paper are confined to one manufacturer only.

For a quality control test a distinction must be made between viable and non-viable cells. This varies amongst manufacturers and can be a result of many factors. In the case of this work, three different battery manufacturers identified excessive self-discharge rate and early capacity fade as non-viable cell faults. Probable causes of cells being identified as non-viable include contamination of the constituent material, mechanical assembly errors or imperfections in the SEI. The aim of the proposed technique is to detect the likelihood of one of these malfunctions at the end of phase 2 of the production process (after thermal and electrical cycling). Physical inconsistencies such as these result in differences in the electrochemical performance of the cells. Indeed, the idealised frequency response shown in Fig. 1 is rarely seen in experimentally measured data. Differences in seemingly identical cells such as elongated semicircles, differences in indicated ESR or asymptotes with differing angles, present themselves as symptoms of the above problems. Variations in the electrical measurements from cell to cell can be used to identify changes within a cell such as decreased capacity, increased cell resistance and state of charge variations [8,9,16,30,31]. Therefore, variations in the impedance response can present themselves as indicators of problems in a non-destructive testing technique [20, 32-34].

A. Impedance response library

In order to indicate that the measured impedance spectrum response of non-viable cells differ from the expected response of viable cells, it is necessary to attain a bench-mark impedance spectrum from which any significant deviations can be described as a non-viable result. A statistically significant sample is therefore required for off-line measurement to create a frequency response library from which a test cell may be compared. The performance of a cell is directly related to how the cell is treated during the charging and discharging process [35]. Therefore, careful provision must be made to ensure the condition of the cells used to form the library is identical to those which would be presented during an on-line test. Additionally, state-of-charge, temperature, and any dynamic influence such as external charging current have a significant impact on the impedance spectrum of Li-ion batteries. Therefore, since the exact state-of-charge (SOC) and temperature of a cell cannot be guaranteed at the point of test the impedance response must be measured at a representative range of SOCs and temperatures to build a comprehensive library. To significantly reduce the required data library size and testing time the cells are assumed to be at rest with no external charging current. Studies have shown that changes to the EIS spectrum can continue to occur for some time after the last charge/discharge event [36]. Therefore, a fixed period of five minutes is imposed during the library data gathering process between a CCCV charge and the EIS measurement.

A library of sample cell data is formed first by determining a representative range for the SOC and temperatures associated with battery production. The production process includes an electrically driven formation of the SEI. This process is automated and therefore results in cells being presented at the QC stage within a relatively small window of SOC. Equally, the environmental conditions of the production line are carefully controlled to avoid contamination during production. Therefore, it can be reasonably assumed that a tight range of SOCs and temperatures will result; for the purposes of this work 40-60 % SOC and 296-299 K are assumed. In practice, this information is strongly influenced by the particular production process; however, it was agreed as a good representation for the industrial partners involved with the work. At rest, a battery's SOC can be calculated by analysis of the SOC vs open circuit voltage (OCV) relationship. An example characteristic, typical of an automotive Li-ion cell, is shown Fig. 3.

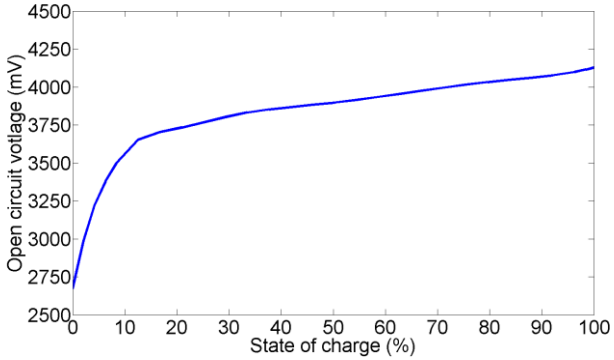

Fig. 3 Example open circuit voltage profile for an automotive Li-ion cell

To avoid mechanical intrusion of the cells it must be assumed that the cells are at thermal equilibrium. This may result in the need to thermally rest cells before the test and cannot be avoided. A temperature measurement can be taken from the cell exterior to determine a value for temperature. For the purposes of this method, the absolute values of temperature and the SOC at which the sampled impedance spectra is measured, are stored in the library. This enables a filtering, normalising and weighted normalising approach to the sample data (these methods are explained in detail below) to create a single target spectrum for any SOC/temperature combination within the bounds of the

library data. A visual representation of the library structure is shown in Fig. 4.

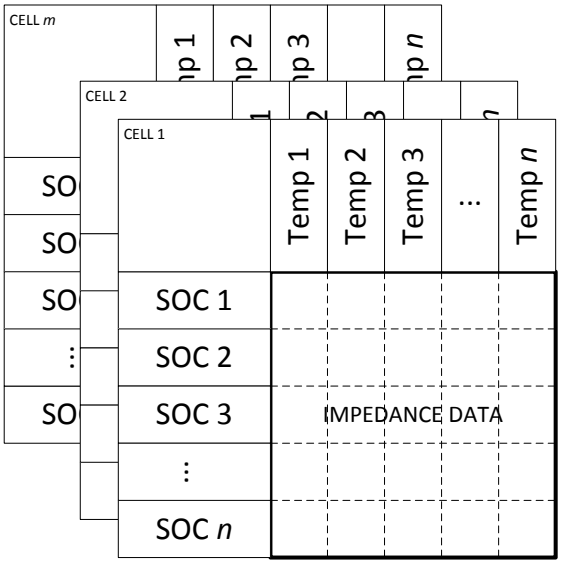

Fig. 4 - Representation of sample data library

B. Data processing and normalisation

In order to generate a projected response the library boundary data must be pre-processed and averaged before being interpolated using weighting factors. Fig. 5 shows the raw EIS plots at a specific temperature and SOC obtained from a batch of eight viable cells from one industrial manufacturer. The raw data shows good coherence in the shape of the plots however there is a discrepancy in the real axis ranging over around 1 mΩ. The similarity in shape and discrepancy in real axis locations represents a dispersion of Ohmic resistance but conservation of reactance response.

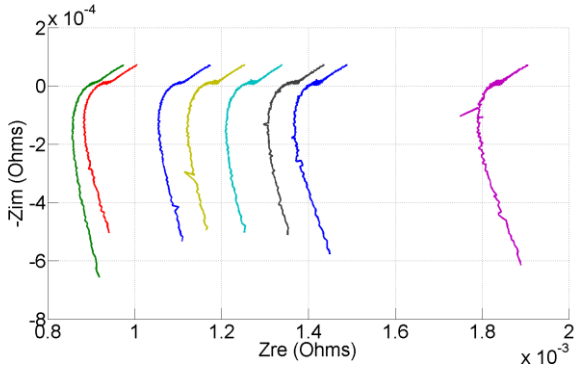

Fig. 5 - Unprocessed EIS plots of eight viable cells

To process this data, and provide an averaged response, all plots are normalised with respect to the real-axis by subtracting a purely real component from each responses. The value of this component is calculated separately for each response separately using the value of the interpolated real-axis crossing point. This value corresponds to the equivalent series resistance discussed in section III.

Variations in the series resistance of cells could be from internal faults, thus where the series resistance deviates significantly from that expected, the cell is considered to be faulty. Small deviations in series resistance, as shown in Fig. 5 (range < 1mΩ), can be considered to arise from variations in the quality of the connection of the probes to the cell tabs.

Removing the series component of the EIS trace at the real axis crossing (i.e. $Z_{im} = 0$) has the effect of shifting each of the plots uniformly in a negative real direction so that they each cross the real-axis at the origin. This 'normalization' is simply a mathematical process to enable an averaging of the shape of the response and is not representative of any physical property of the cell. Each response is then filtered with respect to the frequency-axis to remove noise. For the example shown in Fig. 5 it is found that a simple decimation of the data is generally sufficient to ensure smooth traces for the testing process. In the event of more noisy data, such as may be experienced in a production environment, more complex low-pass filtering of the data with respect to frequency or repeat measurements may be necessary. The resulting 'normalized' and processed profile for the same initial data in Fig. 5 is shown in Fig. 6.

The positive imaginary component of the response (the capacitive region) now shows good correlation between the responses and a mean impedance can be calculated for each frequency point to obtain a single averaged response. This is used as the expected response of a cell at the given SOC and temperature. Importantly, the processed results show a good correlation of difference between the responses of viable and non-viable cells (Fig. 7).

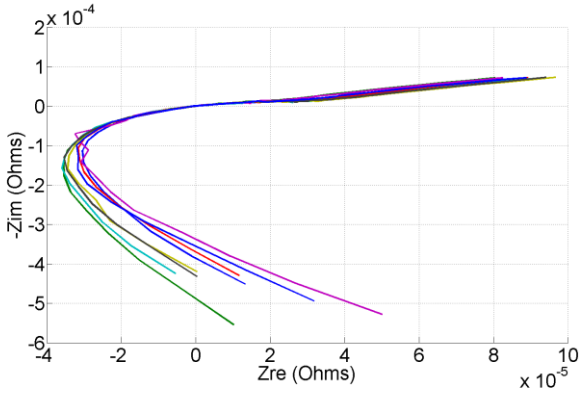

Fig. 6 - Normalised and filtered responses from Fig. 5 data

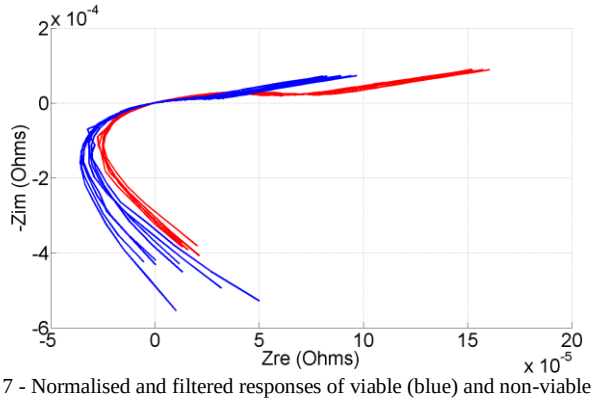

Fig. 7 - Normalised and filtered responses of viable (blue) and non-viable cells (red)

C. Interpolation of library responses

In order to create a target profile, which is a viable cell's projected response based on the library data, the SOC and

temperature of the test cell must be measured. It is then assigned four boundary conditions from the library. Taking the example that the library contains data for SOCs of 40, 45, 50, 55 and 60 % at temperatures of 296, 297, 298 and 299 K and a test cell is measured at 46 % SOC and 297.4 K the four datasets contained within the library which bound the test cell conditions are as follows; (297 K, 45%), (297 K, 50%), (298 K, 45%) and (298 K, 46%). A weighting factor can be assigned to each pair of SOC and each pair of temperature boundaries through a simple proportionality calculation. This process necessarily assumes that between two boundary conditions the relationship is linear. Although the assumption is unlikely to be strictly true, the variation in responses at such tight intervals is small and the assumption is employed here in order to reduce computational complexity (thus improving the test time). In the case of the above example the weighting factor for the SOC pair can be calculated by (4);

$$w_s = \frac{S_{TC} - s}{S - s} = \frac{46 - 45}{50 - 45} = 0.2 \quad (4)$$

where w_s is the weighting factor for SOC, S_{TC} is the measured test cell SOC, S and s are the upper and lower boundary SOCs respectively. An identical approach is used to calculate the temperature weighting factor, w_t (5);

$$w_T = \frac{T_{TC} - t}{T - t} = \frac{297.4 - 297}{298 - 297} = 0.4 \quad (5)$$

where T_{TC} is the measured test cell temperature, T and t are the upper and lower boundary temperatures respectively. The four boundary responses result in four impedance points per frequency. Expressed in a complex plane the four points at each frequency for upper SOC/upper temperature, upper SOC/lower temperature, lower SOC/upper temperature and lower SOC/lower temperature can be expressed as ST, St, sT and st respectively; or represented in a notional graphical way, as shown by Fig. 8.

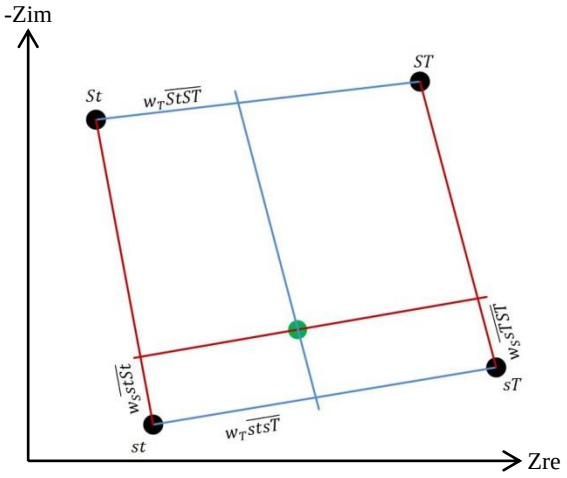

Fig. 8 - Graphical representation of boundary points and intersection vectors

The above procedure is repeated for each frequency point to create an interpolated frequency response for any given SOC and temperature within the library boundaries. The result is the expected response from a viable cell at a specific SOC and temperature. A suitable tolerance margin is then allocated around this response, and this defines the 'acceptable' response for a viable cell. For the cell responses shown in this work a tolerance margin of 12.5μΩ is found to give satisfactory results, however, different cell chemistries require this margin to be tuned accordingly. The size of the tolerance band is derived through sample measurements of viable and non-viable cells. Anything outside the tolerance margin defines a non-viable data point. In this work, at least 80% viable data points is deemed to be a pass result. The process for the test is summarised as a flowchart in Fig. 9.

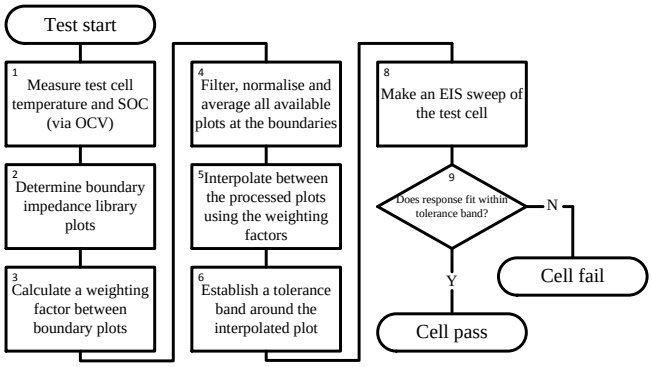

Fig. 9 - Flowchart showing the test procedure

The process shown in Fig. 9 is explained as follows;

1. *Measure test cell temperature and SOC (via OCV).*The potentiostat is used in OCV mode (no charging or excitation current) to measure the cell open circuit voltage and the temperature. Measurements are stored as variables in the data processing algorithms to be used in the next step.
2. *Determine boundary impedance library plots.* The OCV is converted to SOC via the known OCV vs SOC characteristic, as shown in Fig. 3. The SOC and temperature are used to determine the four upper and lower library datasets
3. *Calculate a weighting factor between boundary plots.*The weighting factor is used to determine the interpolation coefficients between the four library datasets. It is determined from the measured SOC and temperature values, and from where they lie between the library dataset measurement conditions
4. *Filter, normalise and average all available plots at the boundaries.* All plots are normalised so that the real axis crossing point is translated in the negative real axis direction so that it crosses at the origin. A low pass filter and decimation process is undertaken to smooth the data out. For the plots shown in this paper, the raw data is clean enough to only employ the decimation process, which is set to be one in eight data points.
5. *Interpolate between the processed plots using the weighting factors.* For each library dataset point, a four way interpolation is performed as discussed in section IV. The result is a predicted profile for the measured SOC and temperature.
6. *Establish a tolerance band around the interpolated plot.* A tolerance band is established around the predicted profile. This is encompassed by taking a radius from each predicted point and then projecting two tangents to the

resulting circles between the two adjacent data points; thus forming a linear corridor between data points.

7. *Make an EIS sweep of the test cell.* An EIS measurement is made at the same frequencies points as those for the predicted profile. The data is stored.
8. *Does response fit within tolerance band?* Each data point is checked to see whether is lies within the established tolerance band established in step 6. If it is within the tolerance band then it is deemed to be a viable data point and the converse if it lies outside. A tally of viable and non-viable measured points is kept. After the sweep a decision is made on the viability of the measured cell based on a threshold percentage of viable measured points to non-measured points.

The normalised, measured EIS responses of five non-viable cells are shown in Fig. 10. It is worth noting, that with respect to Fig. 1, the results in Fig. 10 relate to Section 1 to Section 5; where Section 2 is effectively removed via the real component normalization process. For these cells, the main difference in the viable and non-viable response is in section 5. These are compared to the normalised, averaged interpolated response of a viable cell as calculated using the previously described procedure. The results clearly show a measurable difference between the responses of the non-viable cells and the typical viable cell response; particularly in the low frequency region. This demonstrates the feasibility of using EIS measurements to create a background library, data processing to create a benchmark predicted response and a full EIS sweep in order to differentiate between viable and non-viable cells – the NDT. In the case of the measurements presented in Fig. 10, the response of each of the non-viable cells is shown to be very similar. This being the case, it is reasonable to conclude that the series of non-viable cells potentially have the same failure mode. Therefore, it is possible for the response of the non-viable cells to also be stored in similar library to the viable cells and processed to produce a normalised, averaged response of non-viable cells using the same method previously proposed. With time, a database of known non-viable phenomena can be recorded. Following further research and investigation into repeated behaviour, it is possible to link these characteristics to specific production problems and enhance the QC process.

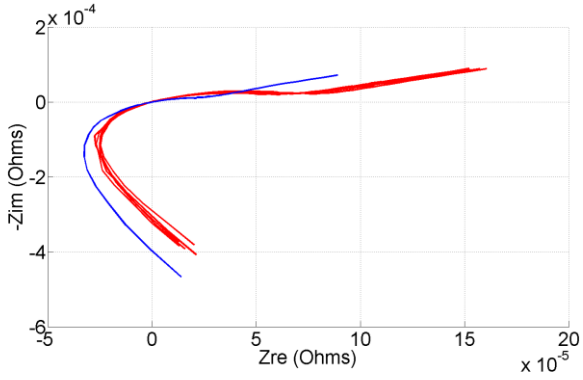

Fig. 10 - Measured response of five non-viable cells (red) and calculated response of viable cells based on empirical library

V. Test Time Reduction Through Frequency Targeting

In this paper, the frequency range in the Nyquist plots (for example Fig. 5) is from 100 mHz to 1 kHz. The measurements taken to create the library database are logarithmically spaced with 100 points per decade made within this bandwidth. As mentioned, the filtering process includes a decimation step which, for the case of all normalised plots shown in this paper is a factor of eight. In total, the amount of time to measure all 400 data points (a single sweep) and to process the results to get the normalised response is around 570 seconds. Considering the target test time for this work is less than 1 min, it is desirable to improve this time further. To achieve this, a method to reduce the number of required measurement points is proposed.

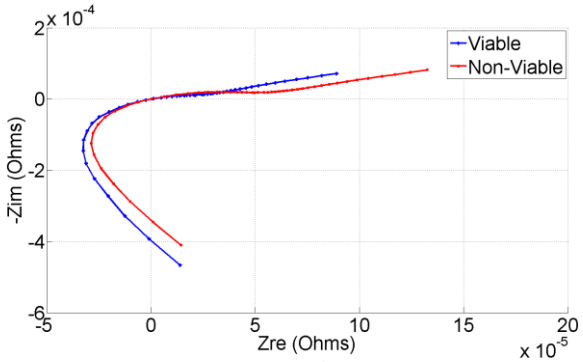

Fig. 11 - Normalised and averaged plots of both viable and non-viable cells

Initially, a full frequency sweep is performed using the aforementioned technique shown in Fig. 9. However, once this has been carried out, it is possible to define an upper and lower frequency limit of interest, which is then used as the basis for all future testing. In this way, the frequency range is reduced and the speed to the test is improved. Importantly, the upper frequency limit is chosen so as to guarantee to be within the positive imaginary plane of the response. This is necessary to ensure that the real-axis intersection point is not omitted from the spectra; this is essential for the aforementioned normalization process. The chosen lower limit is relatively high for typical EIS experiments on such cells. However, the value used reflects the challenging time limit imposed on the NDT procedure. In order to gather a range of impedance readings within a short timespan (<1min) the length of one period of the excitation frequency becomes the key limiting factor. At 100 mHz the period of one test is 10 s and it is common practice for this test to be repeated at least once. Indeed, through research, it is found that a minimum of six readings are required to maximise the robustness of the test. This obviously uses up significant test time to complete, and as a result 100 mHz is the lowest frequency at which six complete measurements can be taken in less than one minute. Therefore, to improve the test time, a frequency targeting approach is devised. In its basic configuration the commercially available potentiostat used is able to make single-sinewave measurements in frequency bands defined by the experimental parameters. A frequency band selection process is then applied by sweeping a window of m frequencies across the entire projected frequency response of both non-viable and viable cells.

Considering a frequency spectrum with n frequency reponses from f_0 to f_n and a frequency window which is m frequencies wide; an array can be constructed to show the mean difference in impedance magnitude between viable and non-viable within the window. If the impedance data arrays are n indexed, the window is m indexed and the resultant averaged array, σ, is A indexed, then the array of average error, σ, where each array location corresponds to a new window location is calculated from (6).

$$\sigma_A = \frac{\sum_{n=A}^{A+m}\left[\left|Z_{V_n}\right| - \left|Z_{NV_n}\right|\right]}{m} \quad (6)$$

where Z_{V_n} and Z_{NV_n} are the derived arrays of projected viable and non-viable responses respectively as described above. After σ is populated it is then sorted by magnitude and the index location of the maximum value element of σ corresponds to the starting frequency index of the measurement window at which the greatest average dispersion of absolute impedance exists in the data set is identified. This window is then used as the frequency target window for use in the online test as it refers to a frequency window where the greatest error between viable and non-viable cells is predicted. The applied frequency range is therefore only m frequencies wide but is targeted at the range of the response at which the deviance is expected to be greatest; this significantly reduces the test time whilst actively searching for the most accurate area of the response.

Impedance magnitude error is selected as viability metric because of the relative ease of calculating a single value error. It is possible to calculate a 2D Cartesian error encompassing real and imaginary impedance error components. Whilst potentially more informative, this increases the complexity of the tolerance banding process. Therefore, the impedance magnitude approach is chosen here for simplicity, and has been found to provide very good discriminative performance. Fig. 12 shows how the test procedure is revised to incorporate this frequency targeting approach.

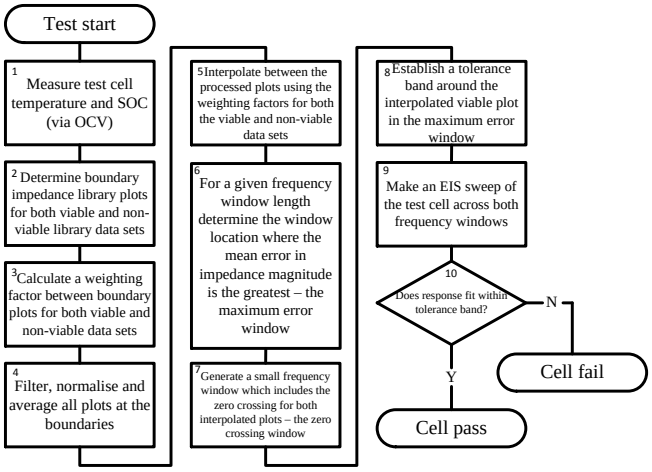

Fig. 12 - Flowchart showing the frequency targeted test procedure

Much of the operation of the targeted approach is similar to that described in section IV with the inclusion of some additional or parallel steps. Relating to Fig. 12;

1. *Measure test cell temperature and SOC (via OCV).* This step is identical to that described above
2. *Determine boundary impedance library plots for both viable and non-viable library data sets.* For this step an identical procedure is undertaken on a library of non-viable data sets to establish a library of boundary data points. This results in eight plots in total, which can be treated as two parallel sets in the same way as the previously described procedure

3–5. *Steps 3 – 5 are performed as per the standard test, but on both viable and non-viable datasets in parallel.*

6. *For a given frequency window length determine the point within the window where the mean impedance magnitude error is greatest – the maximum error window.This step searches for the window location where the average error, calculated by (6), is greatest*
7. *Generate a small frequency window which includes the zero crossing for both interpolated plots – the zero crossing window.* This small window is used to measure the zero crossing point on the test cell so the response of the maximum error window can be normalised with respect to the origin

8-10. *Steps 8 – 10 are performed as per the standard test above but only apply to the maximum error window.*

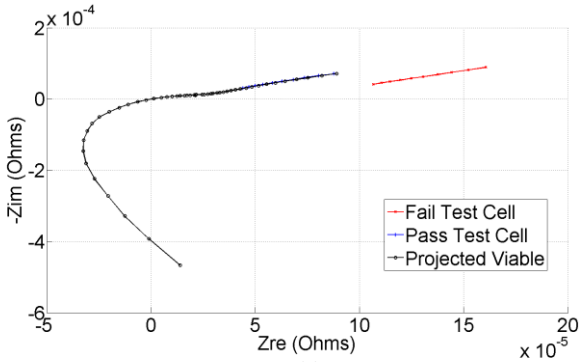

Fig. 13 - Frequency targeted response of failing and passed cell compared with full projected response (test time approx. 55 s/cell, Zero crossing band not shown)

The targeted response of failed and passed cells is shown in Fig. 13. Each is plotted against the projected response of a benchmark viable cell. If the result is inconclusive then a wider window can be attempted or the whole range can be used. This multi-level approach to the testing allows for greater tuning to avoid false results; whilst limiting the test time to a minimum.

VI. Conclusion

Existing methods for automotive Li-Ion battery quality control typically include a self-discharge test in which cells are monitored over a period of several days. After this time, the self-discharge performance is checked to ensure it is within an accepted tolerance. As a result, there is an industrial demand for the development of rapid Li-Ion battery testing techniques to improve the production process. In this paper, a new rapid technique based on Electrochemical Impedance Spectroscopy is proposed to address this issue. The proposed method uses commercially available hardware, and custom software, to create an offline library of impedance data which is used to

benchmark the cell response over a projected range of cell temperatures and SOC. Algorithm development is improved by sampling both viable and non-viable cells, to allow for a novel frequency targeting approach to be taken. This significantly improves the test time. The experimental results, achieved through data processing analysis and optimisation of the frequency targeting approach, validate the efficiency and accuracy of the proposed non-destructive testing technique. Importantly, the proposed state-of-the-art test procedure is shown to accurately distinguish between healthy and faulty cells in less than one minute. Furthermore, due to the reduced test time, it is feasible for the test to be applied to every manufactured cell. This represents a marked improvement over batch type testing techniques. The innovative test is fully non-destructive, a key requirement of the industry, and is independent of any knowledge of the internal chemical mechanisms of the cell.

In this paper, we have proposed a novel end-of-production-line test. The purpose of the test is to rapidly evaluate the viability of a cell immediately after production, so that inferior cells do not enter the field. Future research will focus on how the results of the NDT can be used for specific fault diagnosis, which may inform industry of potential areas of concern in the manufacturing process; such as material defects or contamination. This is not a trivial task, but is an exciting area for further research investigation and collaboration with industry.

ACKNOWLEDGMENT

The authors would like to acknowledge the support of European Commission Framework Seven through the funding of project 285385 (European Lithium-ion Battery Advanced Manufacture – ELIBAMA).

REFERENCES

[1] G. Ablay, "Online Condition Monitoring of Battery Systems With a Nonlinear Estimator," *IEEE Trans. Energy Conv.*, vol. 29, pp. 232-239, 2014.

[2] L. Ee Hui and F. Bodi, "Managing the Complexity of a Telecommunication Power Systems Equipment Replacement Program." *Telecommunications Energy Conference (INTELEC), 2012 IEEE 34th International*, 2012, pp. 1-9.

[3] F. Kramm, "Field experiences with VRLA-gel-batteries in Stationary Applications Over a Period of More Than 20 Years," in *Telecommunications Energy Conference, 2001. INTELEC 2001. Twenty-Third International*, 2001, pp. 603-607.

[4] J. Feng, W. Junwen, L. Jingshan, X. Guoxian, and S. Biller, "Virtual Battery: A Battery Simulation Framework for Electric Vehicles," *Automation Science and Engineering, IEEE Trans on*, vol. 10, pp. 5-15, 2013.

[5] J. Dixon, I. Nakashima, E.F.Arcos, M. Ortuzar, "Electric Vehicle Using a Combination of Ultracapacitors and ZEBRA Battery," *IEEE Trans.Ind. Electron.*, vol.57, no.3, pp.943,949, March 2010

[6] D. I. Stroe, A. I. Stan, R. Teodorescu, "Accelerated Lifetime Testing Methodology for Lifetime Estimation of Lithium-Ion Batteries Used in Augmented Wind Power Plants" *IEEE Trans on Industry Applications* Vol 50 , no. 6, pp 4006 – 4017,2014

[7] A.H. Ranjbar, A. Banaei, A. Khoobroo, B. Fahimi,"Online estimation of state of charge in Li-ion batteries using impulse response concept." *IEEE Trans. Smart Grid*. vol. 3, pp 360–367. 2012.

[8] M. Charkhgard, M. Farrokhi, "State-of-charge estimation for lithium-ion batteries using neural networks and EKF." *IEEE Trans. Ind. Electron*. 57, pp 4178–4187, 2010,

[9] H. Rahimi-Eichi, F. Baronti and M. Chow, "Online adaptive parameter identification and state-of-charge coestimation for lithium-polymer battery cells", *IEEE Trans.Ind. Electron.*, vol. 61, no. 4, pp. 2053-2061, 2014

[10] M. Corno, N. Bhatt, S. M. Savaresi, and M. Verhaegen. "Electrochemical model based state of charge estimation for li-ion cells." *IEEE Trans. Cont. Sys. Tech*, issue 99, 2014.

[11] S. Rodrigues, N. Munichandriah, A.K. Shukla, "AC impedance and state-of-charge analysis of a sealed lithium-ion rechargeable battery." *J. Solid State Electrochem*. 3, 397–405, 1999.

[12] D.V. Do, C. Forgez, K. El Kadri Benkara.; Friedrich, G. "Impedance observer for a Li-ion battery using Kalman filter." *IEEE Trans. Veh. Technol.*, vol.58, pp.3930–3937, 2009.

[13] Y.J. Xing, W. He, M. Pecht, K.L. Tsui "State of charge estimation of lithium-ion batteries using the open-circuit voltage at various ambient temperatures." *Appl. Energy*, 113, pp106–115, 2014

[14] M. Partovibakhsh, G.J. Liu, "An adaptive unscented Kalman filtering approach for online estimation of model parameters and state-of-charge of Lithium-ion batteries for autonomous mobile robots." *IEEE Trans. Control. Syst. Technol.* vol. 23, pp 357–363, 2015.

[15] S. Moura, N. Chaturvedi, and M. Krstic. "Adaptive partial differential equation observer for battery state-of-charge/state-of-health estimation via an electrochemical model." *J. of Dynamic Systems, Measurement, and Control*, no. 136, January 2014.

[16] M. Shahriari and M. Farrokhi, "Online state-of-health estimation of VRLA batteries using state of charge", *IEEE Trans. Ind. Electron*., vol. 60, no. 1, pp. 191-202, 2013

[17] S. Onori, P. Spagnol, V. Marano, Y. Guezennec, and G. Rizzoni. "A new life estimation method for lithium ion batteries in plugin hybrid electric vehicles applications." *Int. J. of Power Electronics*, pp. 302–319, May 2012.

[18] J. Kim, B.H. Cho, "State-of-charge Estimation and state-of-health prediction of a Li-ion degraded battery based on an EKF combined with a per-unit system." *IEEE Trans. Veh. Technol.* 60, pp 4249–4260, 2011,

[19] H. Wang, L. He, J. Sun, S. Liu, F. Wu, "Study on correlation with SOH and EIS model of Li-ion battery." *Proc. 6th Int. Forum on Strategic Technology*, Harbin, China, 22–24, August 2011; pp. 261–264.

[20] M. Gholizadeh and F. R. Salmasi, "Estimation of state of charge, unknown nonlinearities, and state of health of a lithium-ion battery based on a comprehensive unobservable model", *IEEE Trans. Ind. Electron.*, vol. 61, no. 3, pp. 1335-1344, 2014

[21] E. Barsoukov and J. R. Macdonald, *Impedance Spectroscopy: Theory, Experiment, and Applications*: Wiley-Interscience, 2005.

[22] D. Andre, M. Meiler, K. Steiner, C. Wimmer, T. Soczka-Guth, and D. U. Sauer, "Characterization of high-power lithium-ion batteries by electrochemical impedance spectroscopy. I.Experimental investigation" *Journal of Power Sources*, vol. 196, pp. 5334-5341, 6/15/ 2011.

[23] J. L. Morrison and W. H. Morrison, "Real time estimation of battery impedance," in *Aerospace Conference, 2006 IEEE*, 2006, p. 13.

[24] M. D. Levi, K. Gamolsky, D. Aurbach, U. Heider, and R. Oesten, "On electrochemical impedance measurements of LixCo0.2Ni0.8O2 and LixNiO2 intercalation electrodes," *Electrochimica Acta*, vol. 45, pp. 1781-1789, 2/1/ 2000.

[25] J. Vetter, P. Novák, M. R. Wagner, C. Veit, K. C. Möller, J. O. Besenhard, *et al.*, "Ageing mechanisms in lithium-ion batteries," *Journal of Power Sources*, vol. 147, pp. 269-281, 9/9/ 2005.

[26] J. Li, E. Murphy, J. Winnick, and P. A. Kohl, "Studies on the cycle life of commercial lithium ion batteries during rapid charge–discharge cycling," *Journal of Power Sources*, vol. 102, pp. 294-301, 12/1/ 2001.

[27] G. Ning, B. Haran, and B. N. Popov, "Capacity fade study of lithium-ion batteries cycled at high discharge rates," *Journal of Power Sources*, vol. 117, pp. 160-169, 5/15/ 2003.

[28] S. Buller, E. Karden, D. Kok, and R. W. De Doncker, "Modeling the dynamic behavior of supercapacitors using impedance spectroscopy," *IEEE Trans. Ind. Applications*, vol. 38, pp. 1622-1626, 2002.

[29] P. S. Attidekou, S. Lambert, M. Armstrong, J. Widmer, K. Scott, P. A. Christensen, "A study of 40 Ah lithium ion batteries at zero percent state of charge as a function of temperature.", *Journal of Power Sources*, vol.269, pp. 694-703, Dec. 2014.

[30] M. Coleman, L. Chi Kwan, Z. Chunbo, and W. G. Hurley, "State-of-Charge Determination From EMF Voltage Estimation: Using Impedance, Terminal Voltage, and Current for Lead-Acid and Lithium-Ion Batteries," *IEEE Trans. Ind. Electron*., vol. 54, pp. 2550-2557, 2007.

[31] Z. Fei, L. Guangjun, F. Lijin, and W. Hongguang, "Estimation of Battery State of Charge With H Observer: Applied to a Robot for Inspecting Power Transmission Lines" *IEEE Trans. Ind. Electron*., vol. 59, pp. 1086-1095, 2012.

[32] P. Munoz-Condes, M. Gomez-Parra, C. Sancho, M. A. G. San Andres, F. J. Gonzalez-Fernandez, J. Carpio, *et al.*, "On Condition Maintenance Based on the Impedance Measurement for Traction Batteries: Development and Industrial Implementation", *IEEE Trans. Ind. Electron*., vol. 60, pp. 2750-2759, 2013.

[33] R. G. Hoffmann, J. E. Slade, and J. L. Morrison, "Development and test of a real time battery impedance estimation system", in *Aerospace Conference, 2006, IEEE*, pp. 8, 2006.

[34] S. Buller, M. Thele, R. W. A. A. De Doncker, and E. Karden, "Impedance-based simulation models of supercapacitors and Li-ion batteries for power electronic applications", *IEEE Trans. Ind. Applications*., vol. 41, pp. 742-747, 2005.

[35] C. Liang-Rui, C. Jin-Jia, H. Chun-Min, W. Shing-Lih, and S. Deng-Tswen, "Improvement of Li-ion Battery Discharging Performance by Pulse and Sinusoidal Current Strategies", *IEEE Trans. Ind. Electron*.,, vol. 60, pp. 5620-5628, 2013.

[36] W. Waag, S. Käbitz, D. U. Sauer, "Experimental investigation of the lithium-ion battery impedance characteristic at various conditions and aging states and its influence on the application", *Applied Energy*, vol. 102, pp 885-897, ISSN 0306-2619 Feb. 2013,

[37] S. Haghbin, S. Lundmark, M. Alakula, O. Carlson "Grid-Connected Integrated Battery Chargers in Vehicle Applications: Review and New Solution", *IEEE Trans. Ind. Electron*., vol.60, no.2, pp.459-473, Feb. 2013

[38] A. Kuperman, U. Levy, J. Goren, A. Zafransky, A. Savernin, "Battery Charger for Electric Vehicle Traction Battery Switch Station", *IEEE Trans. Ind. Electron*., vol.60, no.12, pp.5391-5399, Dec. 2013

[39] H. Rahimi-Eichi, U. Ojha, F. Baronti, M. Chow, "Battery Management System: An Overview of Its Application in the Smart Grid and Electric Vehicles," in *IEEE Industrial Electronics Magazine*, vol.7, no.2, pp.4-16, June 2013

[40] S. Ebbesen, P. Elbert, L. Guzzella, "Battery State-of-Health Perceptive Energy Management for Hybrid Electric Vehicles," *IEEE Trans. Veh. Technol.*, vol.61, no.7, pp.2893-2900, Sept. 2012

[41] S.J. Moura, J.L. Stein, H.K. Fathy, "Battery-Health Conscious Power Management in Plug-In Hybrid Electric Vehicles via Electrochemical Modeling and Stochastic Control," *IEEE Trans. Control Sys. Tech., IEEE Transactions on* , vol.21, no.3, pp.679,694, May 2013

[42] M. Landi, G. Gross, "Measurement Techniques for Online Battery State of Health Estimation in Vehicle-to-Grid Applications," *IEEE Trans. Instrum.and Meas.*, vol.63, no.5, pp.1224-1234, May 2014